

Secrecy Outage Analysis of Two-Hop Decode-and-Forward Mixed RF/UWOC Systems

Yi Lou, *Member, IEEE*, Ruofan Sun, Julian Cheng, *Senior Member, IEEE*,
Donghu Nie, and Gang Qiao, *Member, IEEE*

Abstract

We analyze the secrecy performance of a two-hop mixed radio frequency (RF)/underwater wireless optical communication (UWOC) system using a decode-and-forward (DF) relay. All RF and UWOC links are modeled by the $\alpha - \mu$ and exponential-generalized Gamma distributions, respectively. We first derive the expressions of the secrecy outage probability (SOP) in exact closed-form, which are subsequently used to derive asymptotic expressions at high SNR that only includes simple functions for further insight. Moreover, based on the asymptotic expression, we can determine the optimal transmit power for a wide variety of RF and UWOC channel conditions. All analyses are validated using Monte Carlo simulation.

Index Terms

Underwater wireless optical communication (UWOC), mixed RF/UWOC system, physical layer security, secrecy outage probability (SOP), performance analysis.

I. INTRODUCTION

Underwater wireless optical communication technology (UWOC) is emerging as an effective solution to the explosive growth of underwater applications [1]. By using blue and green light, which have minimal attenuation when transmitting underwater, underwater optical communication can achieve ultra-high data rates over certain distances.

A two-hop communication system using a single relay is an effective means to extend the communication distance and improve the performance of the communication system. According

to the forwarding mechanism used in the relay, the types of relays can be divided into amplify-and-forward (AF) relay and decode-and-forward (DF) relay.

To enable ultra-high-speed communication across the sea surface between underwater and airborne nodes, RF and UWOC technologies are often used in combination to form so-called hybrid RF/UWOC systems for ultra-high-speed transmissions across the sea surface between underwater and airborne nodes. With an ocean buoy or surface vessel acting as a relay, an RF/UWOC communications system can be conveniently implemented in a two-hop configuration.

Physical layer security has been studied extensively in RF/FSO hybrid communication systems [2]–[4]. Recently, the security issue of hybrid RF/UWOC communication systems has become a hot topic of research. The secrecy performance of two-hop mixed RF/UWOC systems using AF [5] and DF [6] relays are both studied, where the RF channel is modeled using a Nakagami distribution and the UWOC channel is modeled using a mixture exponential-Gamma distribution.

However, some authors have recently proposed a more accurate distribution, i.e., exponential-generalized Gamma (EGG), for modeling UWOC channels through laboratory experiments, which can take into account not only the temperature gradient but also the effect of bubbles on turbulence, for both freshwater and salty water [7]. Further, Nakagami distribution is not general enough to model more realistic physical fading scenarios. The $\alpha - \mu$ distribution is a more flexible channel model that can model more realistic physical scenarios using two distribution parameters, α and μ , to describe the non-linearity of the propagation medium and the number of clusters of multipath waves, respectively [8]. Moreover, The $\alpha - \mu$ distribution can be easily extended to Rayleigh, Nakagami- m , Weibull, one-sided Gaussian, etc., by setting the parameters α and μ to specified values.

This paper is the first to analyze the secrecy performance of a mixed RF/UWOC system using a DF relay, where the UWOC link is modeled using the novel EGG distribution and all the RF links are modeled using the versatile α - μ distributions. We derive the exact closed-expression of the secrecy outage probability (SOP) in terms of bivariate H -functions. Moreover, for further enlightenment and determine the optimal transmitting power, we derive the asymptotic SOP expressions at high SNR that includes only simple functions.

The rest of this letter is organized as follows. In Section II, the channel and system models are presented. In Section III, the end-to-end performance metrics are studied. Numerical results are discussed in Section IV, followed by the conclusion in Section V.

II. SYSTEM AND CHANNEL MODELS

We consider a mixed RF/UWOC system in which the source node (S) in the air transmits its private data to the legitimate destination node (D) located underwater via a trusted DF relay node (R), which can be a buoy or a surface ship. RF channel from source to relay and underwater optical channel from the relay to destination node are assumed to follow $\alpha - \mu$ and EGG distributions, respectively. One unauthorized receiver (E) attempts to eavesdrop on RF signals received by the relay node during transmission.

A. RF channel model

All the RF links are assumed to be block fading and modeled by the $\alpha - \mu$ distribution. The probability density function (PDF) for the instantaneous SNR of SR link (denoted by γ_1) and SE link (denoted by γ_e) are given as $\gamma_k = \frac{P_k}{\sigma_k^2} = \bar{\gamma}_k |h_k|^2$, where $k \in \{1, e\}$, $|h_k|^2$ denotes the instantaneous channel power gain, P_k denotes the transmission power, and σ_k^2 denotes the noise power. γ_k can be expressed as [9]

$$f_{\gamma_k}(\gamma_k) = \frac{\alpha}{\Gamma(\mu)} \frac{\mu^\mu}{(\bar{\gamma}_k)^{\alpha\mu}} \gamma_k^{\alpha\mu-1} \exp\left(-\mu \left(\frac{\gamma_k}{\bar{\gamma}_k}\right)^\alpha\right) \quad (1)$$

where $k \in \{1, e\}$, $\mu \geq 0$, $\alpha \geq 0$, $\gamma_k \geq 0$, and $\Gamma(\cdot)$ is the gamma function. The distribution parameters α and μ dictate the non-linearity and multipath propagation characteristics of the fading model.

Using (26), the complementary cumulative distribution function (CCDF) of γ_1 , i.e., $\bar{F}_{\gamma_1}(\gamma)$ can be derived as follows

$$\begin{aligned} \bar{F}_{\gamma_1}(\gamma_1) &= \int_{\gamma_1}^{\infty} f_{\gamma_1}(\gamma_1) d\gamma_1 \\ &\stackrel{(a)}{=} \int_{\gamma_1}^{\infty} \kappa H_{0,1}^{1,0} \left[\gamma_1 \Lambda \left| \begin{matrix} (-\frac{1}{\alpha} + \mu, \frac{1}{\alpha}) \end{matrix} \right. \right] d\gamma_1 \\ &\stackrel{(b)}{=} -\frac{i\kappa}{2\pi} \int_{\mathcal{L}} \Lambda^{-s} \Gamma\left(\frac{s}{\alpha} + \mu - \frac{1}{\alpha}\right) \int_{\gamma_1}^{\infty} \gamma_1^{-s} d\gamma_1 ds \\ &\stackrel{(c)}{=} \gamma \kappa H_{1,2}^{2,0} \left[\gamma \Lambda \left| \begin{matrix} (0, 1) \\ (-1, 1), (-\frac{1}{\alpha} + \mu, \frac{1}{\alpha}) \end{matrix} \right. \right] \end{aligned} \quad (2)$$

where $\kappa = \frac{\beta}{\Gamma(\mu)\bar{\gamma}_k}$, $\Lambda = \frac{\beta}{\bar{\gamma}_k}$, $\beta = \frac{\Gamma(\mu + \frac{1}{\alpha})}{\Gamma(\mu)}$, and $H_{\cdot,\cdot}^{\cdot,\cdot}[\cdot|\cdot]$ is the H -Function [10, Eq. (1.2)]. Step (a) is derived by using [10, Eq. (1.125)]. Step (b) is obtained by using [11, Eq. (1.1.2)] and

rearranging the integral variables. Step (c) is obtained by solving the integral with respect to x , and using [11, Eq. (1.1.1)] and [11, Eq. (2.1.5)].

B. UWOC channel model

To consider the combined effects of air bubbles and temperature gradients of the UWOC channel on the received optical irradiance in both pure water and salty water, we modeled the UWOC fading using the EGG distribution. The instantaneous SNR D of a IM/DD-based system with OOK modulation is defined as $\gamma_2 = (\eta I)^2 / N_0$, where η is the effective photoelectric conversion ratio, and N_0 denotes the power of noise [7]. the PDF of I can be expressed as [7]

$$f_I(I) = \frac{\omega}{\lambda} \exp\left(-\frac{I}{\lambda}\right) + (1 - \omega) \frac{cI^{ac-1}}{b^{ac}\Gamma(a)} \exp\left(-\frac{I^c}{b^c}\right) \quad (3)$$

where ω is the mixture weight of the EGG distribution, λ is the parameter linked to the exponential distribution, a , b and c are the parameters related to the exponential distribution.

The PDF of the instantaneous received SNR at D can be given as

$$f_{\gamma_2}(\gamma) = \frac{c(1 - \omega)}{\gamma r \Gamma(a)} e^{-\left(\frac{\gamma}{b^r \mu_r}\right)^{\frac{c}{r}}} \left(\frac{\gamma}{b^r \mu_r}\right)^{\frac{ac}{r}} + \frac{\omega}{\gamma \lambda r} \left(\frac{\gamma}{\mu_r}\right)^{\frac{1}{r}} e^{-\frac{1}{\lambda} \left(\frac{\gamma}{\mu_r}\right)^{\frac{1}{r}}}. \quad (4)$$

The CCDF of γ_2 is therefore obtained from [12, Eq. (3.381.3)], and is given as

$$\begin{aligned} \bar{F}_{\gamma_2}(\gamma_2) &= \int_{\gamma_2}^{\infty} f_{\gamma_2}(\gamma_2) d\gamma_2 \\ &= \omega \exp\left(-\frac{1}{\lambda}\right) \left(\frac{\gamma}{\mu_r}\right)^{\frac{1}{r}} - \frac{(\omega - 1)}{\Gamma(a)} \Gamma\left(a, \frac{\gamma^{c/r}}{b^c \mu_r^{c/r}}\right) \end{aligned} \quad (5)$$

where $\gamma(\cdot, \cdot)$ is the upper incomplete Gamma function [12, Eq. (8.350.2)].

III. SOP

An SOP defines the probability of failing to obtain a reliable and secure transmission. SOP is the most commonly used performance metric for evaluating the secrecy performance of communication systems in the presence of eavesdroppers [13], and can be expressed as

$$P_{\text{out}}(R_s) = \Pr\{C_s(\gamma_{eq}, \gamma_e) \leq R_s\}. \quad (6)$$

Referring to [14], the lower bound for the SOP is derived as

$$P_{\text{out}}^L(R_s) \approx \int_0^{\infty} F_{\gamma_{eq}}(\Theta\gamma) f_{\gamma_e}(\gamma) d\gamma$$

where γ_{eq} is the end-to-end instantaneous SNR of the mixed RF/UWOC system using the DF relay, and can be given as follows

$$\gamma_{eq} = \min(\gamma_1, \gamma_2). \quad (7)$$

Using (7), the CDF of the SNR γ_{eq} can be expressed as

$$\begin{aligned} F_{\gamma_{eq}}(\gamma) &= \Pr[\min(\gamma_1, \gamma_2) < \gamma] \\ &= 1 - (1 - F_{\gamma_1}(\gamma))(1 - F_{\gamma_2}(\gamma)) \\ &= 1 - \bar{F}_{\gamma_2}(\gamma)\bar{F}_{\gamma_1}(\gamma). \end{aligned} \quad (8)$$

After substituting (2) and (5) into (7) and some simplification, γ_{eq} can be expressed in the following form

$$\begin{aligned} F_{eq}(\gamma) &= 1 + \frac{\kappa(\omega - 1)}{\Lambda\Gamma(a)} \Gamma\left(a, b^{-c} \left(\frac{\gamma}{\mu_r}\right)^{c/r}\right) \\ &\times H_{1,2}^{2,0} \left[\gamma\Lambda \left| \begin{matrix} (1, 1) \\ (0, 1), (\mu, \frac{1}{\alpha}) \end{matrix} \right. \right] - \frac{\kappa\omega}{\Lambda} \exp\left(-\frac{1}{\lambda} \left(\frac{\gamma}{\mu_r}\right)^{\frac{1}{r}}\right) \\ &\times H_{1,2}^{2,0} \left[\gamma\Lambda \left| \begin{matrix} (1, 1) \\ (0, 1), (\mu, \frac{1}{\alpha}) \end{matrix} \right. \right]. \end{aligned} \quad (9)$$

Using (26) and (9) and after some simplification, SOP_L can be expressed as follows

$$P_{out}^L = 1 + K_1 + K_2 \quad (10)$$

where

$$\begin{aligned} K_1 &= \frac{\kappa(1 - \omega)\alpha_e\kappa_e}{\Lambda\Gamma(a)} \Lambda_e^{\alpha_e\mu_e - 1} \int_0^\infty \exp(-(\gamma\Lambda_e)^{\alpha_e}) \gamma^{\alpha_e\mu_e - 1} \\ &\times \Gamma\left(a, b^{-c} \left(\frac{\gamma\Theta}{\mu_r}\right)^{\frac{c}{r}}\right) H_{1,2}^{2,0} \left[\gamma\Theta\Lambda \left| \begin{matrix} (1, 1) \\ (0, 1), (\mu, \frac{1}{\alpha}) \end{matrix} \right. \right] d\gamma \end{aligned} \quad (11)$$

and

$$\begin{aligned} K_2 &= -\frac{\kappa\omega\alpha_e\kappa_e}{\Lambda} \Lambda_e^{\alpha_e\mu_e - 1} \int_0^\infty \exp\left(-(\gamma\Lambda_e)^{\alpha_e} - \frac{1}{\lambda} \left(\frac{\gamma\Theta}{\mu_r}\right)^{\frac{1}{r}}\right) \\ &\times \gamma^{\alpha_e\mu_e - 1} H_{1,2}^{2,0} \left[\gamma\Theta\Lambda \left| \begin{matrix} (1, 1) \\ (0, 1), (\mu, \frac{1}{\alpha}) \end{matrix} \right. \right] d\gamma. \end{aligned} \quad (12)$$

To obtain a closed expression for SOP, we use H function to express the exponential functions in (11) and (12) as [?, Eq. (07.34.03.0046.01)]

$$\exp(-(\gamma\Lambda_e)^{\alpha_e}) = \frac{1}{\alpha_e} H_{0,1}^{1,0} \left[\gamma\Lambda_e \left| \left(0, \frac{1}{\alpha_e}\right) \right. \right] \quad (13)$$

and

$$\exp\left(-\frac{1}{\lambda} \left(\frac{\gamma\Theta}{\mu_r}\right)^{\frac{1}{r}}\right) = r H_{0,1}^{1,0} \left[\frac{\gamma\Theta\lambda^{-r}}{\mu_r} \left| (0, r) \right. \right]. \quad (14)$$

The Generalized gamma function in (11) is also expressed in the form of H function as [?, Eq. (06.06.26.0005.01)]

$$\Gamma\left(a, b^{-c} \left(\frac{\gamma\Theta}{\mu_r}\right)^{\frac{c}{r}}\right) = H_{1,2}^{2,0} \left[b^{-c} \left(\frac{\gamma\Theta}{\mu_r}\right)^{\frac{c}{r}} \left| \begin{array}{l} (1, 1) \\ (0, 1), (a, 1) \end{array} \right. \right]. \quad (15)$$

$$K_1 = -\frac{\kappa r \omega \kappa_e}{\Lambda \Lambda_e} \left(\frac{\Lambda_e \lambda^r \mu_r}{\Theta}\right)^{\alpha_e \mu_e} H_{1,0;0,1;1,2}^{0,1;1,0;2,0} \left[\begin{array}{l} \frac{\lambda^r \Lambda_e \mu_r}{\Theta} \left| (1 - r\alpha_e \mu_e, r, r) \right. : (1, 1) \\ \lambda^r \Lambda \mu_r \left| \left(0, \frac{1}{\alpha_e}\right) \right. : (0, 1), \left(\mu, \frac{1}{\alpha}\right) \end{array} \right] \quad (16)$$

$$K_2 = -\frac{\kappa(1-\omega)\kappa_e}{\Lambda\Gamma(a)\Lambda_e} H_{1,0;1,2;1,2}^{0,1;2,0;2,0} \left[\begin{array}{l} b^{-c} \left(\frac{\Theta}{\Lambda_e \mu_r}\right)^{\frac{c}{r}} \left| \left(1 - \mu_e, \frac{c}{r\alpha_e}, \frac{1}{\alpha_e}\right) \right. : (1, 1) \quad ; \quad (1, 1) \\ \frac{\Theta \Lambda}{\Lambda_e} \left| \left(0, 1\right), (a, 1) \right. : (0, 1), \left(\mu, \frac{1}{\alpha}\right) \end{array} \right] \quad (17)$$

Then, using the mellin transform of the product of three H -functions [15, Eq. (2.3)], we can obtain the exact closed-form of K_1 and K_2 as in (16) and (17), in terms of bivariate H -function, respectively. Finally, a closed-form expression for SOP can be readily deduced by substituting (16) and (17) into (10). Also note that, bivariate H -function has already been implemented in MATLAB [16], Python [17], and Mathematica [18], and can be easily evaluated.

In order to demonstrate the usefulness of the exact closed-form expression of SOP and gain more insight into the effect of model parameters of the EGG and $\alpha - \mu$ channels on the secrecy performance, we next derive the asymptotic expression for SOP at high SNRs. We consider two scenarios, i.e., $\gamma_1 \rightarrow \infty$ and $\gamma_e \rightarrow \infty$.

We first consider the scenario $\gamma_1 \rightarrow \infty$. Based on the definition of the bivariate H -function, we can rewrite K_1 as

$$K_1 = \frac{\kappa(1-\omega)\kappa_e}{4\pi^2\Lambda\Gamma(a)\Lambda_e} \int_{\mathcal{L}} \int_{\mathcal{L}} \frac{\Gamma(a-s)\Gamma(-s)\Gamma(-t)\Gamma\left(\mu - \frac{t}{\alpha}\right)}{\Gamma(1-s)\Gamma(1-t)} \Gamma\left(\frac{cs}{r\alpha_e} + \mu_e + \frac{t}{\alpha_e}\right) \left(\frac{\Theta\Lambda}{\Lambda_e}\right)^t \left(b^{-c}\Theta^{c/r}\Lambda_e^{-\frac{c}{r}}\mu_r^{-\frac{c}{r}}\right)^s dsdt. \quad (18)$$

Observing that as $\gamma_1 \rightarrow \infty$, $\frac{\Theta\Lambda}{\Lambda_e} \rightarrow 0$, we therefore convert the line integral of t in (18) into the form of the H -function. Then, K_1 can be rewritten as

$$K_1 \approx 2i\pi \frac{\kappa(1-\omega)\kappa_e}{4\pi^2\Lambda\Gamma(a)\Lambda_e} \int_{\mathcal{L}} \frac{\Gamma(a-s)\Gamma(-s)}{\Gamma(1-s)} b^{-cs} \left(\frac{\Theta}{\Lambda_e\mu_r}\right)^{\frac{cs}{r}} \times \underbrace{H_{2,2}^{2,1} \left[\frac{\Theta\Lambda}{\Lambda_e} \left| \begin{matrix} \left(1 - \frac{cs}{r\alpha_e} - \mu_e, \frac{1}{\alpha_e}\right), (1, 1) \\ (0, 1), (\mu, \frac{1}{\alpha}) \end{matrix} \right. \right]}_{\Xi_1} ds. \quad (19)$$

Using [11, Eq. (1.8.4)], Ξ_1 can be asymptotically expanded as the sum of the residues of all poles to the left of the contour, and is given as

$$\Xi_1 \approx \Gamma(\mu)\Gamma\left(\frac{cs}{r\alpha_e} + \mu_e\right) - \frac{1}{\mu} \left(\frac{\Theta\Lambda}{\Lambda_e}\right)^{\alpha\mu} \times \Gamma\left(\frac{cs + r\alpha\mu}{r\alpha_e} + \mu_e\right). \quad (20)$$

After some simplification, we can express K_1 as $\gamma_1 \rightarrow \infty$ into the following form

$$K_1 \approx \left(\frac{\Theta\Lambda}{\Lambda_e}\right)^{\alpha\mu} H_{2,2}^{1,2} \left[b^c \left(\frac{\Lambda_e\mu_r}{\Theta}\right)^{\frac{c}{r}} \left| \begin{matrix} (1-a, 1), (1, 1) \\ \left(\frac{\alpha\mu}{\alpha_e} + \mu_e, \frac{c}{r\alpha_e}\right), (0, 1) \end{matrix} \right. \right] \times \frac{(1-\omega)}{\Gamma(a)\Gamma(\mu+1)\Gamma(\mu_e)} - \frac{(1-\omega)}{\Gamma(a)\Gamma(\mu_e)} \times H_{2,2}^{1,2} \left[b^c \left(\frac{\Lambda_e\mu_r}{\Theta}\right)^{\frac{c}{r}} \left| \begin{matrix} (1-a, 1), (1, 1) \\ \left(\mu_e, \frac{c}{r\alpha_e}\right), (0, 1) \end{matrix} \right. \right]. \quad (21)$$

Similarly, to obtain the asymptotic expression for K_2 as $\gamma_1 \rightarrow \infty$, we first represent K_2 as the following form

$$K_2 = \frac{\kappa r \omega \kappa_e}{4\pi^2 \Lambda} \Lambda_e^{\alpha_e \mu_e - 1} \left(\frac{\Theta \lambda^{-r}}{\mu_r}\right)^{-\alpha_e \mu_e} \int_{\mathcal{L}} \int_{\mathcal{L}} \frac{\Gamma\left(\mu - \frac{t}{\alpha}\right)}{\Gamma(1-t)} \times \Gamma(-t)\Gamma\left(-\frac{s}{\alpha_e}\right)\Gamma(rs + rt + r\alpha_e\mu_e) (\lambda^r \Lambda \mu_r)^t \times \left(\frac{\lambda^r \Lambda_e \mu_r}{\Theta}\right)^s dsdt. \quad (22)$$

Noting that as $\gamma_1 \rightarrow \infty$, $\lambda^r \Lambda \mu_r \rightarrow \infty$, so we rewrite K_2 to the following form

$$K_2 \approx \frac{i\kappa r \omega \kappa_e}{2\pi \Lambda \Lambda_e} \left(\frac{\Lambda_e \lambda^r \mu_r}{\Theta} \right)^{\alpha_e \mu_e} \int_{\mathcal{L}} \Gamma \left(-\frac{s}{\alpha_e} \right) \left(\frac{\lambda^r \Lambda_e \mu_r}{\Theta} \right)^s \times H_{2,2}^{2,1} \left[\lambda^r \Lambda \mu_r \left| \begin{array}{c} (1-r(s+\alpha_e \mu_e), r), (1, 1) \\ (0, 1), (\mu, \frac{1}{\alpha}) \end{array} \right. \right] ds. \quad (23)$$

Using [11, Eq. (1.5.9)], Ξ_2 can be asymptotically expanded as the sum of the residues of all poles to the right of the contour, and is given as

$$\Xi_2 \approx \Gamma(\mu) \Gamma(r(s+\alpha_e \mu_e)) - \frac{1}{\mu} (\Lambda \lambda^r \mu_r)^{\alpha \mu} \times \Gamma(r(s+\alpha \mu + \alpha_e \mu_e)). \quad (24)$$

Substituting (24) into (23) and performing some simplification yields

$$K_2 \approx \frac{r\omega \Lambda^{\alpha \mu}}{\Gamma(\mu+1)\Gamma(\mu_e)} \left(\frac{\Lambda_e}{\Theta} \right)^{\alpha_e \mu_e} (\lambda^r \mu_r)^{\alpha \mu + \alpha_e \mu_e} \times H_{1,1}^{1,1} \left[\frac{\Theta \lambda^{-r}}{\Lambda_e \mu_r} \left| \begin{array}{c} (1, \frac{1}{\alpha_e}) \\ (r(\alpha \mu + \alpha_e \mu_e), r) \end{array} \right. \right] - \frac{r\omega}{\Gamma(\mu_e)} \times \left(\frac{\Lambda_e \lambda^r \mu_r}{\Theta} \right)^{\alpha_e \mu_e} H_{1,1}^{1,1} \left[\frac{\Theta \lambda^{-r}}{\Lambda_e \mu_r} \left| \begin{array}{c} (1, \frac{1}{\alpha_e}) \\ (r\alpha_e \mu_e, r) \end{array} \right. \right]. \quad (25)$$

Following a similar approach to that used in scenario $\gamma_1 \rightarrow \infty$, we can obtain the asymptotic K_1 and K_2 for the scenario when $\gamma_e \rightarrow \infty$ (the detailed derivation is omitted for brevity) as

$$K_1 \approx -\frac{r(1-\omega)\alpha_e}{c\Gamma(a)\Gamma(\mu)\Gamma(\mu_e)} \left(\frac{b^r \Lambda_e \mu_r}{\Theta} \right)^{\alpha_e \mu_e} \times H_{3,3}^{2,2} \left[\frac{b^{-r}}{\Lambda \mu_r} \left| \begin{array}{c} (1, 1), (1-\mu, \frac{1}{\alpha}), (1+\frac{r\alpha_e \mu_e}{c}, \frac{r}{c}) \\ (\frac{r\alpha_e \mu_e}{c}, \frac{r}{c}), (a+\frac{r\alpha_e \mu_e}{c}, \frac{r}{c}), (0, 1) \end{array} \right. \right] \quad (26)$$

and

$$K_2 \approx -\frac{r\omega \alpha_e}{\Gamma(\mu)\Gamma(\mu_e)} \left(\frac{\Lambda_e \lambda^r \mu_r}{\Theta} \right)^{\alpha_e \mu_e} \times H_{2,2}^{1,2} \left[\frac{\lambda^{-r}}{\Lambda \mu_r} \left| \begin{array}{c} (1, 1), (1-\mu, \frac{1}{\alpha}) \\ (r\alpha_e \mu_e, r), (0, 1) \end{array} \right. \right]. \quad (27)$$

It is noted that, as $\gamma_1 \rightarrow \infty$, the first term in both (21) and (25) tends to zero, while the second term tends to a constant related to the quality of both the UWOC and the eavesdropping RF channels, which means that the secrecy outage capacity will be saturated at high transmit

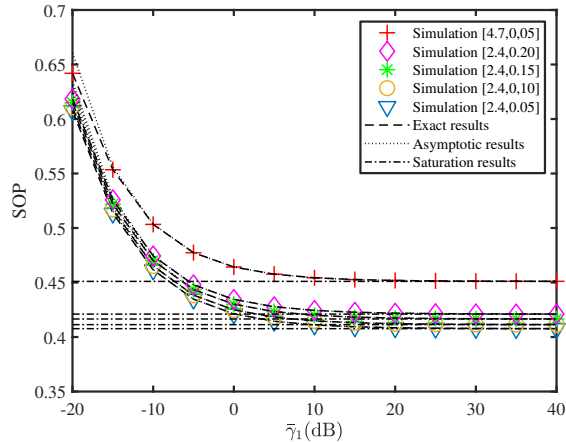


Fig. 1. SOP versus $\bar{\gamma}_1$ with various UWOC parameters and $\alpha = \alpha_e = 1.2$, $\mu = \mu_e = 0.5$, $R_s=0.5$, and $\bar{\gamma}_e = \bar{\gamma}_2 = -20$ dB.

power γ_1 . In the next section, the simulation results will again confirm this theorem. Also, the expression consisting of the second terms of (21) and (25) are also drawn together in the simulation, using saturation results as the legend.

IV. NUMERICAL RESULTS AND DISCUSSION

In this section, we use Monte-Carlo simulations to verify the correctness of exact closed-form expressions and asymptotic expressions. Furthermore, by varying the parameter values of the $\alpha-\mu$ and the EGG models, we thoroughly investigate the relationship between the secrecy performance of the mixed RF/UWOC system and propagation medium non-linearity and the number of multipath clusters in the RF channel, and the temperature gradient and air bubbles in the UWOC channel. For simplicity, we use $[\cdot, \cdot]$ to represent the values of [air bubbles level, temperature gradient] in this section.

Fig. 1 varies the exact and asymptotic expressions of SOP against the SNR of SR link γ_1 over the two-hop mixed RF/UWOC system with various UWOC parameters. The average SNR of the UWOC channel is fixed to $\bar{\gamma}_2 = -20$ dB. The parameters of the UWOC channels for scenarios 1 to 4 are [2.4, 0.05], [2.4, 0.10], [2.4, 0.15], [2.4, 0.20], and [4.7, 0.05], respectively. The SE and SR channels have the same parameters, i.e., $\alpha = \alpha_e = 1.2$ and $\mu = \mu_e = 0.5$. As shown in the figure, analytical and simulation results well match to each other. Moreover, when the SNR is between -20 dB and 10 dB, the SOP decreases as the SNR increases. However, from 10 dB onwards, the SOP is saturated, which confirms the claims of the theorem in the last paragraph of Section III. Then, from the point of view of energy efficiency, one should use the transmission

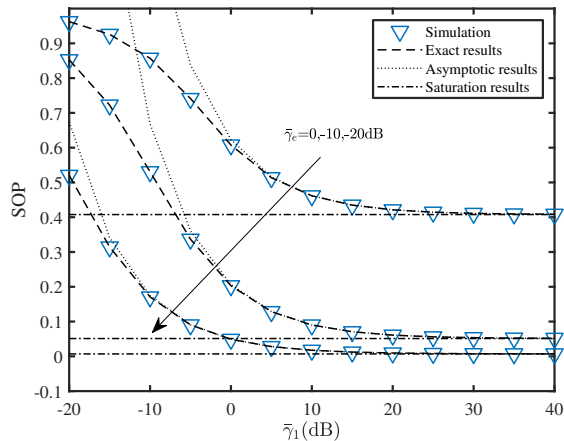


Fig. 2. SOP versus $\bar{\gamma}_1$ with various $\bar{\gamma}_e$ and UWOC parameters [2.4, 0.05], $\alpha = \alpha_e = 1.2$, $\mu = \mu_e = 0.5$, and $\bar{\gamma}_2 = -20$ dB.

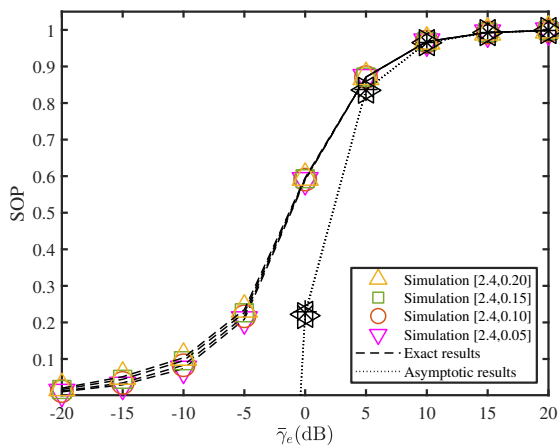


Fig. 3. SOP versus $\bar{\gamma}_e$ with various UWOC parameters and $\alpha = \alpha_e = 0.9$, $\mu = \mu_e = 1.5$, $R_s = 0.5$, $\bar{\gamma}_1 = 30$ dB, and $\bar{\gamma}_2 = 0$ dB.

power corresponding to the saturation starting point. For example, with a UWOC parameter of [4.7, 0.05], the corresponding optimal transmission power is 10 dB for the value of SOP equals to 0.45. Further, when the quality of the UWOC channel is better, the SOP is smaller. Actually, increasing the quality of the UWOC channel while keeping the quality of the eavesdropping link unchanged increases the overall capacity of the two-hop system, thereby increasing the SOP.

Fig. 2 uses the same parameters as in Fig. 1, except that only the parameters of the UWOC channel in scenario 1 are used, and the average SNR of the eavesdropping channel γ_e is -20 dB, -10 dB, and 0 dB, respectively. As shown in the figure, when the quality of the SE channel is better, the saturation value of the SOP is larger and vice versa. In addition, the asymptotic

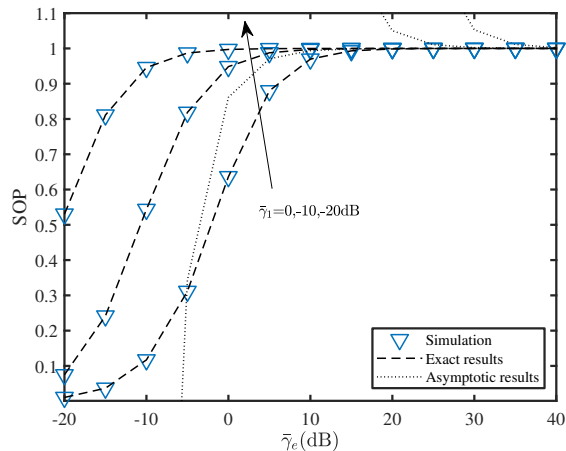


Fig. 4. SOP versus $\bar{\gamma}_e$ with various $\bar{\gamma}_1$ and UWOC parameters [2.4, 0.05], $\alpha = \alpha_e = 0.9$, $\mu = \mu_e = 1.5$, and $\bar{\gamma}_2 = 0$ dB.

results are very accurate from 0 dB, while the saturation results give a correct indication of the saturation value for each scenario.

Fig. 3 varies the exact and asymptotic expressions of SOP against the SNR of SE link $\bar{\gamma}_e$ with fixed $\bar{\gamma}_1 = 30$ dB and various UWOC parameters. The other parameters are the same as in Fig. 1. The same principles that explain the curves in Fig. 1 also apply to explaining the curves in Fig. 3.

Fig. 4 uses the same parameters as in Fig. 2, except that $\bar{\gamma}_2 = 0$ dB and γ_e is -20 dB, -10 dB, and 0 dB, respectively. From the figure, we can observe that when the SE link quality is fixed, the better the SR link quality, the smaller the value of SOP at -20 dB and the larger the corresponding SNR value as SOP increases to 1.

V. CONCLUSION

We considered the secrecy performance of a mixed RF/UWOC system, where the EGG distribution is used for modeling the UWOC channel and $\alpha - \mu$ distribution is used for model RF links for legitimate and eavesdropping users. We derived the exact closed-form and asymptotic expressions of the secrecy outage probability and investigated the effect of channel quality on the SOP performance.

REFERENCES

- [1] Z. Zeng, S. Fu, H. Zhang, Y. Dong, and J. Cheng, "A Survey of Underwater Optical Wireless Communications," *IEEE Commun. Surv. Tutor.*, vol. 19, no. 1, pp. 204–238, 1st Quart., 2017.

- [2] H. J. Lei, H. Zhang, I. S. Ansari, C. Gao, Y. C. Guo, G. F. Pan, and K. A. Qaraqe, "Performance Analysis of Physical Layer Security Over Generalized-K Fading Channels Using a Mixture Gamma Distribution," *IEEE Commun. Lett.*, vol. 20, no. 2, pp. 408–411, Feb. 2016.
- [3] H. Lei, Z. Dai, K. Park, W. Lei, G. Pan, and M. Alouini, "Secrecy outage analysis of mixed RF-FSO downlink SWIPT systems," *IEEE Trans. Commun.*, vol. 66, no. 12, pp. 6384–6395, Dec. 2018.
- [4] H. J. Lei, H. L. Luo, K. H. Park, Z. Ren, G. F. Pan, and M. S. Alouini, "Secrecy Outage Analysis of Mixed RF-FSO Systems With Channel Imperfection," *IEEE Photonics J.*, vol. 10, no. 3, pp. 1–13, Jun. 2018.
- [5] E. Illi, F. El Bouanani, D. B. Da Costa, F. Ayoub, and U. S. Dias, "Dual-Hop Mixed RF-UOW Communication System: A PHY Security Analysis," *IEEE Access*, vol. 6, pp. 55 345–55 360, 2018.
- [6] E. Illi, F. El Bouanani, D. Benevides da Costa, P. C. Sofotasios, F. Ayoub, K. Mezher, and S. Muhaidat, "Physical Layer Security of a Dual-Hop Regenerative Mixed RF/UOW System," *IEEE Trans. Sustain. Comput.*, pp. 1–1, 2020.
- [7] E. Zedini, H. M. Oubei, A. Kammoun, M. Hamdi, B. S. Ooi, and M. S. Alouini, "Unified Statistical Channel Model for Turbulence-Induced Fading in Underwater Wireless Optical Communication Systems," *IEEE Trans. Commun.*, vol. 67, no. 4, pp. 2893–2907, Apr. 2019.
- [8] M. D. Yacoub, "The α - μ Distribution: A Physical Fading Model for the Stacy Distribution," *Ieee T Veh Technol*, vol. 56, no. 1, pp. 27–34, Jan. 2007.
- [9] L. Kong, G. Kaddoum, and H. Chergui, "On Physical Layer Security Over Fox's H-Function Wiretap Fading Channels," *IEEE Trans. Veh. Technol.*, vol. 68, no. 7, pp. 6608–6621, Jul. 2019.
- [10] A. M. Mathai, R. K. Saxena, and H. J. Haubold, *The H-Function Theory and Applications*, ser. Book. New York, NY, USA: Springer, 2010.
- [11] A. A. Kilbas and M. Saigo, *H-Transforms: Theory and Applications (Analytical Method and Special Function)*, 1st ed., ser. Book. CRC Press, 2004.
- [12] I. S. Gradshteyn and I. M. Ryzhik, *Table of Integrals, Series, and Products*, 7th ed., ser. Book. San Diego, CA, USA: Academic Press, 2007.
- [13] W. Research., "The wolfram functions site," 2020. [Online]. Available: <http://functions.wolfram.com>
- [14] H. J. Lei, Z. J. Dai, I. S. Ansari, K. H. Park, G. F. Pan, and M. S. Alouini, "On Secrecy Performance of Mixed RF-FSO Systems," *IEEE Photonics J.*, vol. 9, no. 4, pp. 1–14, Aug. 2017.
- [15] P. K. Mittal and K. C. Gupta, "An integral involving generalized function of two variables," *Proc. Indian Acad. Sci. - Sect. A*, vol. 75, no. 3, pp. 117–123, 1972.
- [16] H. Chergui, M. Benjillali, and M.-S. Alouini, "Rician K-factor-based analysis of XLOS service probability in 5G outdoor ultra-dense networks," *IEEE Wirel. Commun. Lett.*, 2018.
- [17] H. R. Alhennawi, M. M. H. El Ayadi, M. H. Ismail, and H. A. M. Mourad, "Closed-Form Exact and Asymptotic Expressions for the Symbol Error Rate and Capacity of the H-Function Fading Channel," *IEEE Trans. Veh. Technol.*, vol. 65, no. 4, pp. 1957–1974, Apr. 2016.
- [18] F. D. Almeida Garcia, A. C. Flores Rodriguez, G. Fraidenraich, and J. C. S. Santos Filho, "CA-CFAR Detection Performance in Homogeneous Weibull Clutter," *IEEE Geosci. Remote Sens. Lett.*, vol. 16, no. 6, pp. 887–891, 2019.